Nanoparticle geometrical effects on percolation, packing density, and magnetoresistive properties in ferromagnet-superconductor-insulator nanocomposites

Xiangdong Liu,[1,*] Raghava P. Panguluri,[1] Rupam Mukherjee,[1,†] Debabrata Mishra,[1,‡] Shiva Pokhrel,[1] Daniel P. Shoemaker,[2,§] Zhi-Feng Huang,[1,‖] and Boris Nadgorny[1,¶]

[1]*Department of Physics and Astronomy, Wayne State University, Detroit, Michigan 48201, USA*

[2]*Materials Department and Materials Research Laboratory, University of California, Santa Barbara, California 93106-5121, USA*

(Received 17 August 2022; accepted 8 November 2022; published 19 December 2022)

The influence of nanoparticle geometrical and percolation effects on the electrical transport and magnetotransport properties of the system are investigated in a number of binary networks composed of superconducting (MgB_2), ferromagnetic (CrO_2 or $La_{1/3}Sr_{2/3}MnO_3$), and insulating ($LiCoO_2$ or Cr_2O_3) nanoparticles. For all-metal CrO_2/MgB_2 binary composites an anomalously high resistance state with two distinct percolation thresholds is found within a narrow range of the constituent composition, as a result of the strong suppression of heterointerfacial conductance between superconducting and half-metallic (CrO_2) nanoparticles and an unexpectedly large value of the percolation threshold of MgB_2. The latter can be attributed to the geometric mismatch between the constituent nanoparticles and the related particle packing and excluded volume effects. The filling factor in this binary composite attains a maximum near the same percolation threshold and exhibits a power-law scaling behavior, which would indicate another geometric phase transition. The geometric effect of constituent particles is also verified through the large changes of percolation threshold in different types of combinations of binary components. Interestingly, the percolation transitions in these binary nanocomposites, either in the case of single or double percolation, are found to be governed by an unconventional scaling behavior of resistance just below the percolation threshold, due to mechanisms determined by heterogeneous interfaces of particles that are absent in conventional single-component percolation systems. In addition, magnetotransport is investigated in CrO_2/MgB_2 junctions, demonstrating nonhysteretic low-temperature magnetoresistance at the half-metal/Type II superconductor interface with the highest values around 42% at liquid helium temperatures obtained at volume fraction between the two percolation thresholds. The results show large variations of magnetoresistance that are highly sensitive to the constituent composition and the sample temperature near the percolation thresholds, demonstrating the interrelation between the structural or geometrical property of the system and materials functionality.

DOI: 10.1103/PhysRevB.106.224417

I. INTRODUCTION

Composite materials, enabling new, intelligently tailored functionalities, are becoming increasingly important in numerous applications. These new functional materials might require various combinations of different constituents [1]. Many properties of these complex materials can be described by the classical percolation models, which serve as a powerful tool for understanding composite systems where geometric phase transitions occur [2]. Percolation effects governing various properties of these materials have been extensively investigated in various complex systems, such as metal-insulator [3] and superconductor-insulator composites [4,5], polymer blends [6], polycrystalline materials [7,8], ferromagnetic [9], and dielectric materials [10].

At the same time, there are many important questions beyond the traditional percolation paradigm that need to be addressed, such as the extent to which the particle shape and size and the nature of conductance between constituent particles in a composite network influence its percolation threshold and scaling exponents. Moreover, for nanoparticle tunneling the geometric properties and electrical connectivity are often not the same among individual particles. While in the case of single-valued two-particle resistance that results from tunneling conductance in a composite system, the universality is believed to be preserved, the most general case of percolation tunneling with variable coupling strength may be nonuniversal [11].

A nontrivial variant of this problem involves percolation in two-component composite systems built solely of

*Present address: Department of Physics, Changchun University of Science and Technology, Changchun City, Jilin Province 130022, China.

†Present address: Department of Applied Physics, School of Chemical Engineering and Physical Sciences, Lovely Professional University Punjab, Phagwara 144411, India.

‡Present address: Department of Physics and Astrophysics, University of Delhi, Delhi 110007, India.

§Present address: Department of Materials Science and Engineering and Materials Research Laboratory, University of Illinois at Urbana-Champaign, Illinois 61801, USA.

‖huang@wayne.edu

¶nadgorny@physics.wayne.edu

conducting nanoparticles, where the geometric property of the system (percolation thresholds) and its electrical property (conductivity) are fully decoupled. This is the case of CrO_2/MgB_2 composites, for example, in which the conductance between individual particles of different conducting components (CrO_2 and MgB_2, each of metallic conductivity) is effectively blocked, leading to an effective insulating region between the individual percolation thresholds of the two components [12]. The reduced interparticle conductivity in this system is increasingly pronounced at lower temperatures, below the superconducting critical temperature of MgB_2 due to the confluence of tunneling effects and the suppression of Andreev refection at the CrO_2/MgB_2 half-metal/superconductor interface [13]. These effects are directly responsible for the double percolation transition observed in this system, resulting in a conductor-insulator-superconductor crossover behavior [12]. Each of the CrO_2- and MgB_2-dominated percolative transitions is fundamentally different from the conventional percolation for a single type of particles involving conducting or superconducting state, resulting in a similar but different form of scaling behavior for the sample resistivity in the vicinity of each percolation threshold when $p < p_c$ (instead of the standard $p > p_c$) in this unconventional binary composite system, as will be further addressed in this work.

Moreover, in ferromagnetic (F)-superconducting (S) nanoparticle composites the property of percolation may be even more complicated, affected by particle interactions, which can be both direct (via dipoles from magnetic nanoparticles) and indirect (via proximity effect). The latter is an example of proximitized materials [14], in which electrical, magnetic, and other properties of heterostructures for various functionalities can be tailored or enhanced. When interactions between constituents is present in a composite system, as examined in this work, additional degrees of freedom for the study of percolation become available, leading to a nonuniversal scaling behavior. Such is the case with magnetic nanoparticles, where spin-dependent transport plays an important role and the system behavior can be characterized by magnetoresistance as well. In the case of CrO_2 nanoparticles, the intrinsic magnetoresitance, which is fairly small, is significantly enhanced by the presence of a nanometer-size dielectric surface layer [9,15], resulting in a tunneling conductance between individual grains. At lower temperatures the effect is further amplified due to the presence of a Coulomb gap, with the maximum magnetoresistance at 5 K being approximately 30% for a pure CrO_2/CrO_2 system and ∼50% for a CrO_2/Cr_2O_3 composite system [16,17]. Importantly, in the latter case the maximum of magnetoresitance is near the percolation threshold [16], which implies a direct correlation between magnetoresistive and percolative properties. In contrast to this well-studied problem [18], the maximum of magnetoresistance in the CrO_2/MgB_2 system corresponds to the maximum interfacial area between CrO_2 and MgB_2 nanoparticles, as found in this study, indicating a different magnetoresistance mechanism, where an effective area of a Type II two-gap superconductor (MgB_2) is reduced due to the magnetic field penetration in the form of Abrikosov vortices with a substantial core size [19]. Somewhat surprisingly, while large magnetoresistance has been observed in F/S and F/S/F junctions based on spin-charge separation and nonequilibrium spin density in superconductors [20], in F/I/S junctions with two zero-field orthogonal magnetization states [21], and in triplet superconductivity devices [22], to the best of our knowledge, direct magnetoresistance measurements in Ferromagnet/Type II superconductor junctions have not been performed thus far.

To study some of these questions in detail, we designed and fabricated a number of hybrid nanocomposites by combining half-metallic ferromagnets, superconductors, and insulating nanoparticles at different volume ratios. This allows us to investigate the connection between percolation effects and the electrical, magnetotransport, and occupational properties of the composites. In our previous work we introduced a double percolation effect [12], manifesting itself as two independent percolative transitions in the composite system, one for a superconducting MgB_2 [23] and the other for a half-metallic CrO_2 [24] network. Correspondingly, we have identified two percolation thresholds for the conductivity of each component, with the one for MgB_2 being anomalously high. We argued that the constituent particle geometric shape and size play a crucial role in achieving the necessary conditions enabling the observation of the double percolation effect. The effect of particle geometry is further studied here by replacing the high aspect ratio ferromagnetic CrO_2 particles by approximately spherical $La_{1/3}Sr_{2/3}MnO_3$ (LSMO) particles [25], or by replacing the spherical-type MgB_2 particles by large cylindrical-shape $LiCoO_2$ ones, for either of which a much lower percolation threshold is then found.

In this paper, we provide the compendium of results on a variety of composite systems with large geometric disparity (including MgB_2/CrO_2, MgB_2/Cr_2O_3, MgB_2/LSMO, and $CrO_2/LiCoO_2$ nanocomposites), which include not only the electrical transport data, but also the detailed measurements of magnetotransport as well as the determination of filling or packing factors. An unconventional scaling behavior for the system resistance [i.e., $R \propto (p_c - p)^{\mu}$] is identified for binary composites, including both cases of double and single percolation in the regime involving heterogeneous particle interfaces, intrinsically different from the property of conventional single-particle-type percolation. The property of particle filling factor, particularly the power-law behavior near the percolation threshold, and effects of excluded volume are investigated. Also identified are the previously unexplored effects of large superconductor-ferromagnet magnetoresistance, which show high variations with the change of sample composition and temperature, particularly in the region between the percolation thresholds, indicating the correlation between geometric and functional properties of the binary composite system.

II. EXPERIMENTS

Sample preparation and structural characterization

A series of ferromagnetic-superconducting composite samples were fabricated by using the traditional cold-pressed technique. CrO_2 and LSMO powders were the two different ferromagnetic components, while MgB_2 was the common superconducting component. In a separate experiment we combined CrO_2 nanoparticles with insulating (at 200 K) $LiCoO_2$ nanoparticles. In our experiments we used

commercial CrO_2, MgB_2, and $LiCoO_2$ powders, whereas LSMO powders were obtained from sintered crystallized pellets. For the latter, hydrated acetates of manganese, lanthanum, and strontium had been mixed in deionized water at 80 °C and stirred until the liquid evaporated. The resulting powder was calcined in air at 1000 °C for 1 h, then allowed to cool to room temperature and pressed into pellets at 17 MPa. The calcined pellets were sintered at 1500 °C for 16 hours with heating and cooling rates of 10 and 20 °C/min, respectively. High firing temperatures (>1200 °C) were required to achieve proper oxygenation and a metal-insulator transition near room temperature. Powder x-ray diffraction (Philips X'Pert with Cu-Kα radiation) was performed and Rietveld analysis using the XND software package [26] confirmed the sample to be phase-pure $La_{1/3}Sr_{2/3}MnO_3$. The two ferromagnet/superconductor components were mixed according to their weight ratios; the mixed powder was then ground in a glass mortar for one hour. As the surface of all of the constituents can be easily oxidized, to obtain reproducible results it was necessary to perform this process in a controlled environment, with the humidity kept below 30%. The ground powder was then compressed at 10 GPa in a hydraulic press into 5-mm-diameter and approximately 1-mm-thick pellets. Immediately after the fabrication, gold wires were attached to the pellet with silver paste. The sample was then mounted on a physical property measurement system (PPMS) puck for transport and magnetotransport measurements. The PPMS excitation current of 2 μA (with the voltage limit of 5 mV) was used for most resistance measurements. The pellet resistance was measured in the temperature range from 2 to 300 K; the magnetoresistance was measured in the magnetic fields of up to 5 T.

For the MgB_2/CrO_2 system, a total of 23 samples were prepared according to the weight fraction x of CrO_2: $x = 0$, 0.1, 0.25, 0.29, 0.31, 0.32, 0.33, 0.34, 0.35, 0.36, 0.365, 0.37, 0.375, 0.38, 0.39, 0.40, 0.41, 0.42, 0.45, 0.5, 0.6, 0.8, and 1. Using the bulk densities of CrO_2, $\rho_1 = 4.89$ g/cm^3, and of MgB_2, $\rho_2 = 2.57$ g/cm^3, weight fractions x can be converted to volume fractions p via

$$p = \frac{x/\rho_1}{x/\rho_1 + (1-x)/\rho_2} = \frac{1}{1 + (\rho_1/\rho_2)(1/x - 1)}. \quad (1)$$

Similar conversion can be used for LSMO- and $LiCoO_2$-based composite systems. To measure packing fractions of the composites, pellets of pure component as well as composite pellets (near the percolation thresholds) were prepared. The packing fraction for a two-component composite was determined with the known bulk densities of CrO_2, LSMO, MgB_2, and $LiCoO_2$ using the following expression:

$$f = \frac{m}{V}\left(\frac{x}{\rho_1} + \frac{1-x}{\rho_2}\right), \quad (2)$$

where m and V are the total mass and volume of the composite pellet which are determined for each composition.

A different geometry was used to determine the interface properties and the contact resistance of MgB_2/CrO_2 particles. In this experiment we first prepared a sample consisting of only one type of powder, cold-pressing it using the same conditions and in the same geometry as for other composite samples. Upon placing the other type of powder on top of this fabricated sample, we cold-pressed them together one more time to form a pellet with a well-defined interface between these two different components.

Composite samples of different compositions were characterized by scanning electron microscopy (SEM). The average size and shape of the particles, as well as their size distribution, were determined from the analysis of the respective SEM images, with the spatial distribution of the two types of particles monitored by energy dispersive x-ray spectroscopy (EDS) as in Ref. [12]. The MgB_2 particles are approximately spherical, with average diameter $D \sim 500$ nm. In contrast, the CrO_2 particles are rodlike, with typical length $L \sim 300$ nm and width $d \sim 40$ nm. The LSMO particles characterized by SEM were also approximately spherical with a polydispersed size distribution ranging from 1 to 5 μm. The majority of $LiCoO_2$ particles, however, can be described as cylindrical, with height about 5–10 μm and diameter about 3–4 μm. $(LSMO)_x(MgB_2)_{1-x}$ composite samples were fabricated via the same technique as the $(CrO_2)_x(MgB_2)_{1-x}$ samples.

III. RESULTS AND DISCUSSIONS

A. Double percolation effect in CrO_2/MgB_2 system

To study the percolative transition in CrO_2/MgB_2 binary composites, electrical characterization was conducted for samples with variable compositions. First, several basic configurations were tested, including a pure CrO_2 sample, a pure MgB_2 sample, and a sandwich-like sample composed of a CrO_2 and a MgB_2 layer separated by an interface. The corresponding R versus T curves are shown in Figs. 1(a), 1(b), and 1(c), respectively. The maximum resistance of a pure CrO_2 and a pure MgB_2 samples is approximately 55 Ω (at $T = 2$ K) and 0.04 Ω (at 300 K), respectively, with the superconducting transition of MgB_2 occurring at $T_C \approx 37$ K. Note that while the residual resistivity of CrO_2 is on the order of ≈5 $\mu\Omega$cm, which corresponds to the mean free path of about 100 nm [18], the low temperature conductivity of pure cold-pressed CrO_2 samples as well as the observed temperature dependence is fully determined by the inter-particle contacts between individual CrO_2 particles.

However, the sample with CrO_2/MgB_2 interface junction has the maximum resistance close to 1000 Ω at 2K, which is approximately 20 times higher than that of the pure CrO_2 sample at this temperature (MgB_2 is superconducting below T_C). While the real atomic interface between MgB_2 and CrO_2 should be rough and coarse, this measurement presented in Fig. 1(c) indicates that the interface resistance between two different types of particles (CrO_2/MgB_2) is approximately an order of magnitude higher than that between the same type of particles (CrO_2/CrO_2 or MgB_2/MgB_2). This conclusion is also consistent with the results obtained from the low-temperature magnetoresistance data near the percolation threshold (see Sec. III E), which shows a much smaller contribution of the CrO_2/CrO_2 interfaces to magnetoresistance as compared to the CrO_2/MgB_2 ones.

Having obtained these results for simplified systems, which have important implications for further analysis and discussion, we focus on cold-pressed $(CrO_2)_x(MgB_2)_{1-x}$ samples of variable compositions. The outcomes of resistance

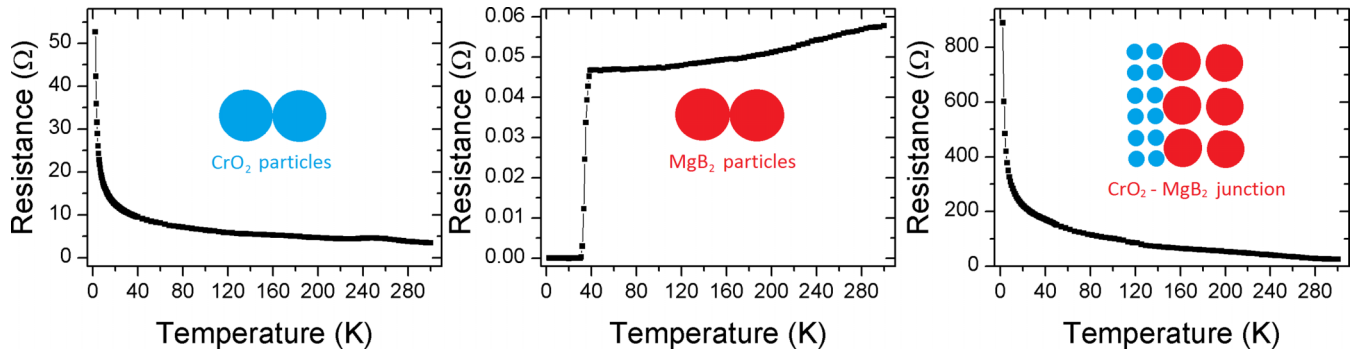

FIG. 1. Temperature-dependent resistance of nanoparticles. Left: Cold-pressed CrO_2 sample; middle: Cold-pressed MgB_2 sample; right: Cold-pressed sandwich-like sample with an interface between CrO_2 and MgB_2.

measurements as a function of temperature across the full range of sample compositions are summarized in Fig. 2. These resistance plots can be categorized into two types: For the samples with high MgB_2 concentration (i.e., small volume fraction p), their R versus T relation is similar to that of pure MgB_2, either superconducting or having very low resistances below a certain temperature, and the values of resistance become generally larger as the MgB_2 volume fraction $1 - p$ decreases (see the first seven panels in Fig. 2). The sample resistance is plotted as a function of volume fractions p at different temperatures in Fig. 3. Note that the resistance does not increase monotonically with the increase of CrO_2

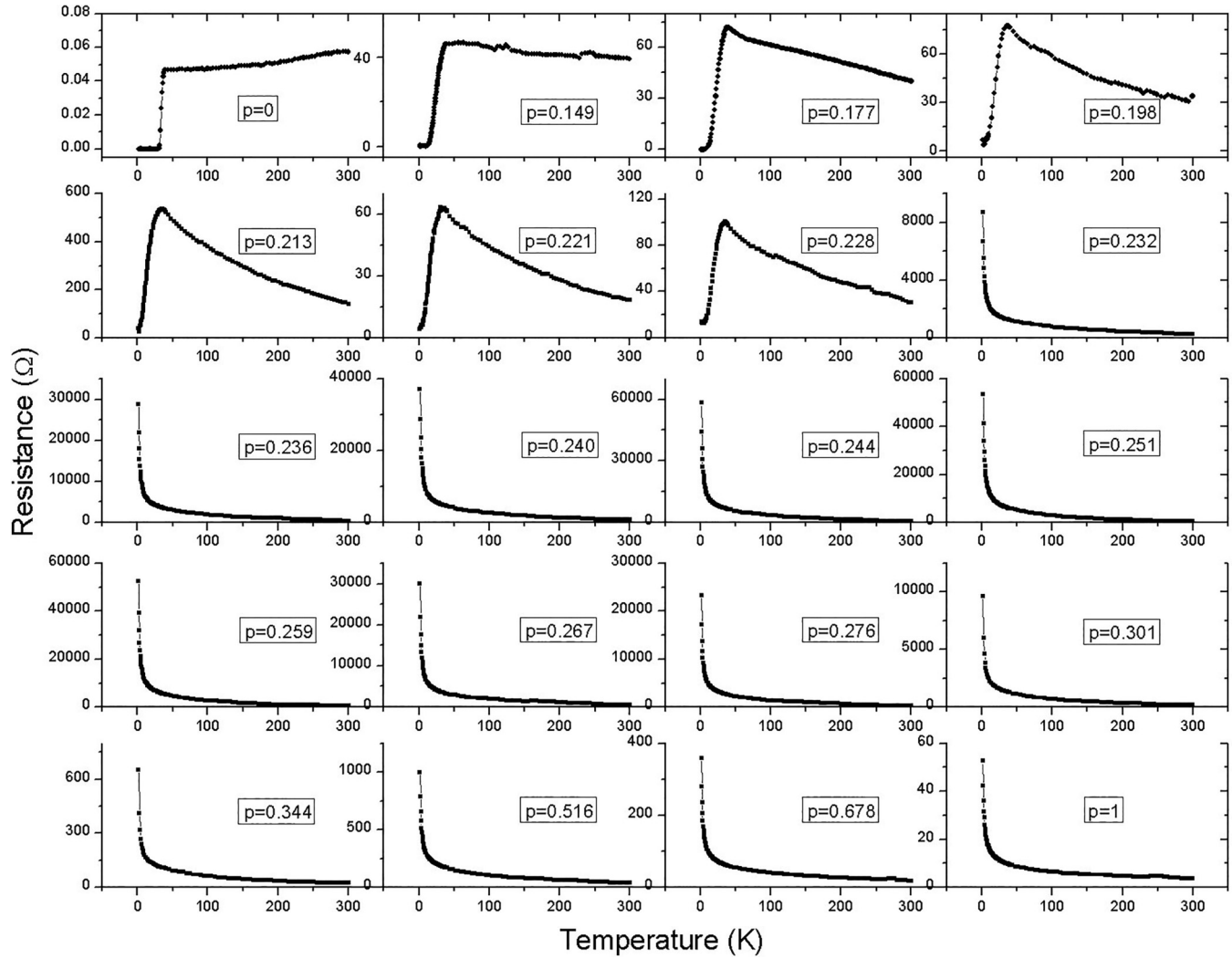

FIG. 2. Sample resistance as a function of temperature for 20 different CrO_2/MgB_2 composites with volume fraction p of CrO_2 ranging from 0 to 1.

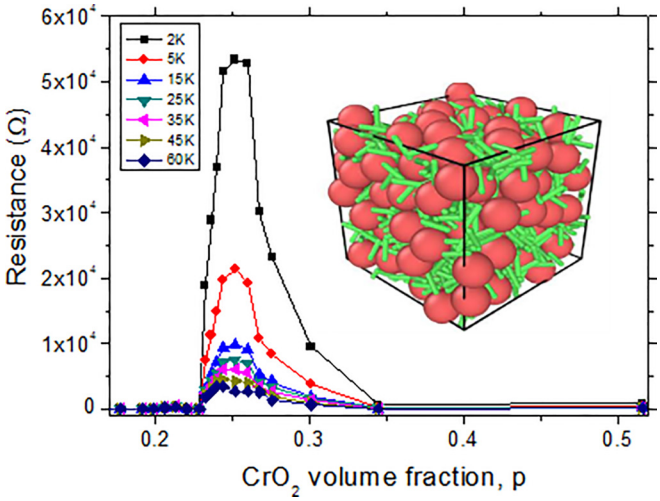

FIG. 3. Resistance of $(CrO_2)_p(MgB_2)_{1-p}$ cold-pressed composites as a function of volume fraction p of CrO_2 at temperatures ranging from 2 to 60 K. Inset: A 3D rendition of $(CrO_2)_p(MgB_2)_{1-p}$ composites.

volume fraction. While the resistance on the MgB_2-rich side ($0 < p < 0.22$) is very low and the resistance on CrO_2-rich side ($0.34 < p < 1$) is also fairly low, the resistance of the composite samples attains peak values within a narrow intermediate range of $0.22 < p < 0.34$. At low temperatures the maximum value of the resistance is about three orders of magnitude higher than that of the pure CrO_2 sample. For example, at 2K the maximum resistances are 450 Ω for $p < 0.22$, 900 Ω for $p > 0.34$, but close to 55 kΩ for $p = 0.25$.

We can attribute this unusual behavior to a distinct double percolation effect appearing in this type of nanocomposite system. As has been shown in Ref. [12], it involves the development of two separate uncorrelated percolative networks with conductive or superconductive paths, and with different percolation thresholds for the two constituents: $p_c^{CrO_2} \approx 0.34$ and $1 - p_c^{MgB_2} \approx 1 - 0.78 = 0.22$. The substantial difference between the values of these two thresholds indicates that the corresponding percolation transitions are not symmetric, a direct consequence of significant asymmetry in the size and shape of the constituent particles, as will be discussed below. Note that the *I-V* characteristics of the composites measured in the range from 0.5 to 100 μA are nonlinear and have a complex temperature dependencies below the critical temperature of MgB_2, particularly near the percolation thresholds. The detailed analysis of this behavior is beyond the scope of this paper.

To explain these surprising results, we recall that the resistance of the heterogeneous interface (i.e., CrO_2/MgB_2) is at least an order of magnitude larger than that of the homogeneous ones (i.e., CrO_2/CrO_2 or MgB_2/MgB_2), particularly at low temperatures, as shown in Fig. 1. Therefore, it is reasonable to assume that in the samples of variable compositions the path maximizing the overall interface region between MgB_2 and CrO_2 clusters would maximize the sample resistance. In this binary composite system two independent percolative transitions have been observed, one from an insulating state to a conductive state (on the CrO_2-rich side) and the other from an insulating state to a superconductive state (on the MgB_2-rich side), which are realized at certain compositions of CrO_2 (or MgB_2). If, in the range of intermediate compositions, none of the two constituent clusters percolate (which, as we will discuss below, requires certain conditions to be satisfied), one can expect the maximized heterointerface and hence maximum resistance somewhere in this range (as seen in Fig. 3), and thus the double percolation effect [12].

In the standard percolation theory, for a system exhibiting a percolative transition the resistance R near the percolation threshold p_c can be expressed by a power law $R \propto (p - p_c)^{-\mu}$ or $R \propto (p - p_c)^s$, where the critical exponent (μ or s) depends on the dimensionality and the intrinsic conducting property (i.e., conducting or superconducting) of the system. For three-dimensional (3D) networks, the critical exponents of insulator-conductor transitions are known to be $\mu \approx 2$ for 3D lattice [27] and $\mu \approx 2.38$ for continuum percolation (as in the Swiss-cheese model) [28], while for a conductor-superconductor transition the expected value of the exponent is $s \approx 0.75$ [29]. However, there is an important difference between the binary nanocomposite system studied here and the conventional conducting-insulating percolation transition with conducting particles embedded in an insulating medium or vacuum. In the latter case, the resistivity is infinite when $p < p_c$ since there is no conducting path, and becomes finite when $p > p_c$ due to the appearance of percolative clusters of conducting particles, with the scaling behavior $R \propto (p - p_c)^{-\mu}$ describing the region of $p > p_c$. In contrast, our binary composite system consists of two types of metallic nanoparticles that are cold-pressed and fill most of the space (subjected to $f < 1$ filling factors); thus, there is always a conducting path available to go through the particles (albeit of different types), with the unfilled space irrelevant in terms of resistivity. In other words, the percolation transition described here refers to the appearance of percolative clusters of one particle type, while the whole composite cluster of both particle types is always percolative. An important feature of this system is that either type of constituent particles (e.g., pure CrO_2 or MgB_2) is conducting or superconducting, while the interface resistance between different species (i.e., CrO_2/MgB_2) is at least an order of magnitude higher as described above (see Fig. 1). When $p > p_c$ with the existence of percolative clusters of a pure constituent particle type such as CrO_2, the resistivity is low and mostly composition-independent (showing as a near-constant value similar to the bulk state). However, once $p < p_c$, no single percolative CrO_2 cluster exists, and the system conducting path would always involve heterogeneous (CrO_2/MgB_2) particle interfaces. While theoretically the resistance of an idealized half-metal/superconductor interface with a delta-function scattering potential may approach infinity at $T = 0$ K [13,30], in reality it generally leads to a finite, albeit orders-of-magnitude increase of resistivity in the superconducting state, moderated by nonzero spin-flip probabilities at the S/F interface due to magnetic impurities [31] or spin-orbit scattering [32], as well as possible differences in the scattering potential strength for majority and minority carriers [33]. Importantly, though, the resistivity reaches its maximum at the largest number of heterogeneous interfaces (i.e., maximum total perimeter of either pure CrO_2 or MgB_2 clusters).

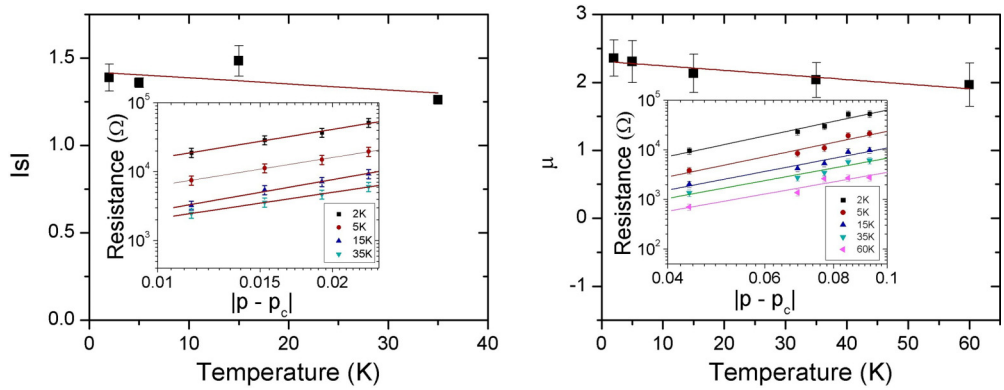

FIG. 4. Temperature dependence of the critical exponents s and μ for the superconductor-insulator and conductor-insulator transitions, respectively. Lines are linear fits. Insets: Resistance scaling near the percolation thresholds at different temperatures. Left: MgB_2-rich side, with $p_c^{MgB_2} = 0.78$; Right: CrO_2-rich side, with $p_c^{CrO_2} = 0.34$. The percolation thresholds are determined as inflection points of R vs p curves.

Hence, here we encounter a new type of percolation transition for binary composites, with the percolation threshold p_c determined by the point at which the resistivity of the sample starts to increase significantly (corresponding to the disappearance of percolative single-type clusters). When $p > p_c$, the conventional behavior of $R \propto (p - p_c)^{-\mu}$ for conductor-insulator transition would not apply since the resistivity corresponds to the constant bulk value as described above. Here the new feature occurs in the region of $p < p_c$ as the resistivity then increases with larger deviation from p_c (i.e., with $|p - p_c|$ increasing). To our knowledge, there has not been any theoretical work available so far for this new type of percolation behavior. However, it would be natural to assume a similar power-law behavior of

$$R \propto |p - p_c|^{\mu}, \tag{3}$$

for this region of $p < p_c$ with conducting paths involving heterogeneous interfaces, as verified by our experimental data for MgB_2/CrO_2 composite (see Fig. 4) and single-percolation systems such as $CrO_2/LiCoO_2$ (see Fig. 7 in Sec. III D below). A similar argument can be applied to the case of conductor-superconductor transition (on the MgB_2 side), with the critical exponent μ replaced by s in Eq. (3).

To demonstrate that the two transitions in our composite systems are governed by the above scaling law, we calculate the values of exponents s and μ at different temperatures, as presented in Fig. 4, and show the log-log plots of resistance versus volume fraction for both transitions, at $p_c^{MgB_2} = 0.78$ for the MgB_2 side of the transition and at $p_c^{CrO_2} = 0.34$ for the CrO_2 side, in the insets of Figs. 4(a) and 4(b), respectively. A close examination of the data confirms that for both MgB_2- and CrO_2-dominated networks the transitions are percolative, with the average exponent $\mu \approx 2.16 \pm 0.15$ (for the insulating-conducting transition on the CrO_2 side) and $s = 1.37 \pm 0.05$ (for the insulating-superconducting transition on the MgB_2 side). Note that the standard deviation for the critical exponent μ is appreciably higher for the CrO_2 side, and there is some weak temperature dependence of μ, varying from 1.97 at 60 K to 2.36 at 2 K, which may be related to the fact that conductance across the CrO_2 percolative network, especially at the lowest temperatures, is dominated by tunneling. Interestingly, these experimental values of critical exponent μ for the conducting-insulating transition on the CrO_2 side, as obtained in this unconventional double percolation system, are very close to the known theoretical values in conventional single-component percolation systems (which are between 2 and 2.38 for 3D lattice and continuum networks, respectively). Whether this is merely a coincidence or indicates the universal behavior of conducting-insulating transition would be of interest for further theoretical or experimental exploration, but is beyond the scope of this work. However, the exponent on the MgB_2 side deviates significantly from the known theoretical result ($s \approx 0.75$) for the conductor-superconductor transition [29], which could be related to the fact that the transition observed here is effectively an insulator-superconductor one (see Fig. 3).

The question of whether the critical exponent s measured in our system should coincide with the one in a conventional conductor-superconductor transition is nontrivial. Indeed, the conductor-superconductor transition can be modeled by short circuiting an element in the resistor model [34], while adding a link between the elements would correspond to the metal-insulator transition (on the metal side). However, in our binary system it is impossible to separate these two operations. Additionally, the critical currents across the MgB_2/MgB_2 interface are likely to be nonuniform and determined not by the properties of the bulk MgB_2, but rather by the properties of interfaces, i.e., the weak links between the MgB_2 particles (although these "weak" links are actually quite strong [35]). In other words, the superconducting current would propagate via the proximity or Josephson coupling between grains, which assumes that the metal-insulator percolative transition should occur first. This is consistent with our measured exponent ($s = 1.37$), which deviates from the value of conventional conductor-superconductor transition toward that of the conductor-insulator transition. Moreover, it is entirely possible that magnetic CrO_2 particles may affect the superconductivity of MgB_2 nanoparticles near the percolation threshold, particularly in view of "surface aging" reported for some of the MgB_2 nanoparticles [36]. In other words, there could be a significant difference between superconductors percolating in a noninteractive media, and in a media with highly localized magnetic moments, as has been shown for

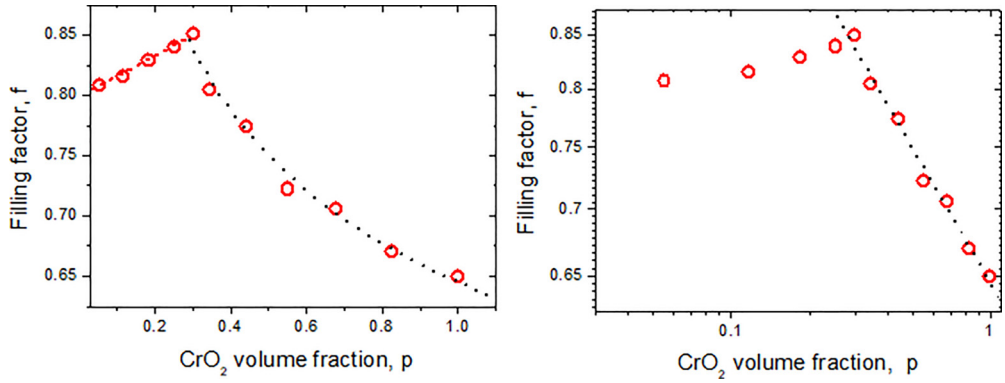

FIG. 5. Filling factor f as a function of volume fraction p across the full range of compositions. Left panel: Linear scale; right panel: Log-log scale, with the slope of the dashed line giving a power-law exponent $\alpha = -0.22$.

CrO_2 particles [37]. If this, indeed, is the case, the critical exponent is likely to scale with the particle size in a nontrivial way, particularly when the interaction length becomes comparable with the nanoparticle size, a phenomenon that could be explored in the future work.

Another difference in our findings, compared to the previously reported results, is the location of percolation thresholds in the heterogeneous nanocomposites studied here. While the observed percolation threshold for CrO_2 ($p_c^{CrO_2} = 0.34$) was close to the known theoretical limit, the threshold for MgB_2 ($p_c^{MgB_2} = 0.78$) was significantly higher than expected. This surprising result, which is strongly dependent on the geometric shape and size disparity of the constituent particles, is key to understanding the double percolation effect. As determined from the SEM images, the length of the individual CrO_2 rodlike particles is only about one half the size of the MgB_2 particles; they are also very thin, with the average aspect ratio about 6.5, so that their volume is around 0.5% of that of MgB_2 spheres. Thus, the percolation of small CrO_2 nanoparticles can be approximated as a percolation process in a continuum matrix. The threshold value of $p_c^{CrO_2}$ is also very close to $p_c = 0.31$ that was recently determined both theoretically and experimentally for a system of conducting and insulating spherocylinders with the same aspect ratio of 6.5 [38], corresponding to the dimensions of CrO_2 particles used here. However, the situation for the percolation of large MgB_2 particles is much more complicated, and involves the particle filling and packing factors as well as the excluded volume effect, as will be outlined below.

B. Composition dependence and power-law behavior of filling factor

For a more comprehensive picture of percolation in the CrO_2/MgB_2 binary system it is also useful to consider the effect of packing density near the percolation threshold. Strictly speaking, it is the spacial occupation or the probability fraction (the product of the volume fraction by the filling factor), rather than the volume fraction itself, that determines the percolation threshold. However, as it turned out, the filling factor reaches a maximum of approximately 85% between the two thresholds. It keeps very close to this value (~82.5% and ~81% at the CrO_2 and MgB_2 thresholds, respectively) and changes only marginally in the range of interest, $0.2 < p < 0.35$, as shown in Fig. 5. Moreover, as the two types of constituent particles have very different sizes and shapes, the filling or packing may have generated some composition-dependent spatial nonuniformity, which would further complicate the estimates of the occupation probability.

In addition to measuring the filling factor near the percolation thresholds, we have investigated its behavior over the whole composition range (see Fig. 5). Interestingly, the maximum of the filling factor appears to be close to the percolation threshold for CrO_2, a nontrivial result. Moreover, while on the MgB_2-rich side (with small $p < p_c^{CrO_2}$ starting from pure MgB_2), the filling factor depends approximately linearly on the volume fraction (up to $p \approx 0.3$; see the left panel of Fig. 5), on the other side of the threshold there is a clearly identifiable power-law dependence with the exponent $\alpha = -0.22$ (see the right panel of Fig. 5). This thus indicates a geometric phase transition associated with particle packing near the percolation threshold, which can be understood qualitatively. Indeed, adding more CrO_2 particles to the already closely packed MgB_2 spheres of variable sizes increases the filling factor—being approximately proportional to the volume fraction p of CrO_2—until, near the threshold for CrO_2 percolation, large finite-size clusters of CrO_2 particles begin to develop, making it no longer possible to position the particles between MgB_2 spheres, and thus driving the filling factor down (toward the filling factor of pure CrO_2, which is much lower). The observation of a power-law behavior at the CrO_2 concentrations beyond the percolation threshold is intriguing, as it may indicate the link between electric (conductive) and geometric properties of the composite system.

Taking $p_c^{MgB_2} = 0.78$ as the value of volume fraction, we convert it to the spacial occupation or probability fraction [39], $P_c^{MgB_2} = f_1 p_c^{MgB_2}$, where f_1 is the filling factor of all the particles at the MgB_2 threshold. Based on the experimental value of MgB_2, i.e., $f_1 = 0.811$, we obtain $P_c^{MgB_2} = f_1 p_c^{MgB_2} = 0.633$, which is within the close packing limit of 0.64 for the random packing of hardcore spheres [40]. Similarly, at $p_c^{CrO_2} = 0.34$, the spacial occupation is given by $P_c^{CrO_2} = f_2 p_c^{CrO_2} = 0.27$ (where f_2 is approximately 0.79), in good agreement with the percolation limit in 3D continuous models ($p_c \approx 0.28$ for 3D continuum percolation [2]).

While the result of $P_c^{MgB_2} = 0.633$ is more reasonable than $p_c^{MgB_2} = 0.78$ which was obtained purely from the value of

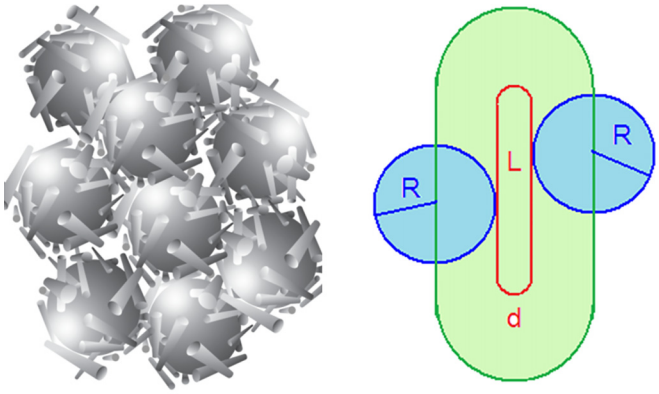

FIG. 6. Left: Schematics of MgB_2 spherical particles caged by CrO_2 thin rods. Right: Excluded volume of a system composed of a sphere (e.g., MgB_2 particle) and a thin rod (e.g., CrO_2 particle).

volume fraction, we need to consider that our samples are cold-pressed, which should further reduce the average distance between the adjacent particles. Hence the value of P_c is expected to be much lower than the random packing limit and be around the range of 0.2–0.5 as found in previous experiments of MgB_2 [8] and $YBa_2Cu_3O_7$ [41] superconductor systems or granular metal films [42], as well as in our measurements of other systems that will be described in Sec. III D. To address this discrepancy, we need to examine the detailed configuration of packing between particles of large geometric contrast, which is related to the effects of excluded volume examined below.

C. Excluded volume effects

As illustrated in Fig. 6, voids between large MgB_2 spheres are very effectively filled by small CrO_2 sticks that are short and paper-thin, particularly under the cold-pressing experimental condition, leading to the high packing density as shown in Fig. 5. These CrO_2 sticks can very effectively screen, or "cage" larger MgB_2 spheres, as can be also seen from the calculation of excluded volume in a sphere-stick system [43,44]. The excluded volume of a given object is defined as the volume around the object into which the center of another object cannot penetrate (both objects are considered to be perfectly rigid) [44,45]. According to Onsager's result for two spherocylinders with diameters D and d and lengths L and l, both randomly oriented, the excluded volume is given by [43,44]

$$V_{\rm ex} = \frac{\pi}{6}(d+D)^3 + \frac{\pi}{4}(d+D)^2(l+L) + \frac{\pi}{4}(d+D)lL. \tag{4}$$

For the sphere-stick system considered here, one of the spherocylinders in Eq. (4) is a sphere (MgB_2) with $l = 0$ and diameter D, while the other is a thin stick (CrO_2) with length L and diameter $d \ll D$, as illustrated in Fig. 6. Thus, from Eq. (4) the excluded volume of this binary composite is simplified as

$$V_{\rm ex} = \frac{\pi}{6}D^3 + \frac{\pi}{4}D^2L. \tag{5}$$

Our measurement of this MgB_2/CrO_2 system yields $L \approx D/2$ (see Sec. II), and thus $V_{\rm ex}/V_{\rm MgB_2} \approx 7/4$, where $V_{\rm MgB_2} = \pi D^3/6$ is the volume of MgB_2 spheres. The percolation threshold for MgB_2 can be approximated as

$$P_c = \frac{N_c V_{\rm MgB_2}}{V_{\rm sys}}, \tag{6}$$

where $V_{\rm sys}$ is the total volume of the system and N_c is the number of MgB_2 spheres at the percolation threshold, which can be estimated from the simplest model [46] as $N_c \approx V_{\rm sys}/V_{\rm ex}$. Substituting this estimation into Eq. (6), we obtain $P_c \approx V_{\rm MgB_2}/V_{\rm ex} \approx 4/7 = 0.57$, which is consistent with our experimental value of $P_c = 0.633$. Note that the percolation threshold is very sensitive to the particle shape and size. For example, paper-thin rectangular particles with a volume fraction close to zero would be extremely efficient in caging the spheres, resulting in the percolation threshold approaching 1.

D. Single percolation in MgB_2/Cr_2O_3, MgB_2/LSMO, and $CrO_2/LiCoO_2$ composites

Since the above explanation of anomalously high percolation threshold for MgB_2 based on the concept of excluded volume is essential for understanding our results, we have performed several additional experiments to confirm that the value of threshold for MgB_2 is, indeed, independent of the double percolation effect *per se*. First, we annealed CrO_2 particles under vacuum using the recipe of Refs. [16,17] to convert them to Cr_2O_3 to study the MgB_2/Cr_2O_3 system. While now we no longer observe double percolation in this system (as Cr_2O_3 particles are insulating), the value of percolation threshold for MgB_2 is found to be practically unchanged (0.76 as compared to 0.78), which confirms our assumption that it is, indeed, the specific large geometric contrast between MgB_2 and Cr_2O_3 or CrO_2 that drives the threshold higher.

In the second experiment we measured the threshold for a MgB_2/LSMO composite system, in which the shape and size of the LSMO particles are quite different from Cr_2O_3 or CrO_2—they are close to spherical but larger in diameter than MgB_2 particles, with much less degree of geometric contrast. Again, for this system only one percolation threshold was observed (as the LSMO particles are insulating) with $p_c^{\rm MgB_2}$ in the range between 0.32 and 0.39, a much smaller percolation threshold compared to the case of MgB_2 particles percolating through the CrO_2 matrix, but very close to the $p_c^{\rm CrO_2} \approx 0.34$ for the CrO_2 percolating network in the spherical MgB_2 matrix. We note that the percolation threshold in the system of insulating-conducting Cr_2O_3/CrO_2 spherocylinders (i.e., with no geometric contrast of constituent particles) was recently determined to be ≈0.31 [38], also quite close to the threshold value obtained here.

The third experiment of CrO_2 percolating network in the $CrO_2/LiCoO_2$ composite is instructive because $LiCoO_2$ particles are also approximately cylindrical (or elliptical) with the diameter of about 3–4 μm and the height of about 10 μm, much larger than the CrO_2 particles. In Fig. 7 we plot the resistance of the $CrO_2/LiCoO_2$ composite as a function of the volume fraction p of CrO_2 and also as a function of $|p - p_c|$ for $p < p_c$ (where the conducting path involves the

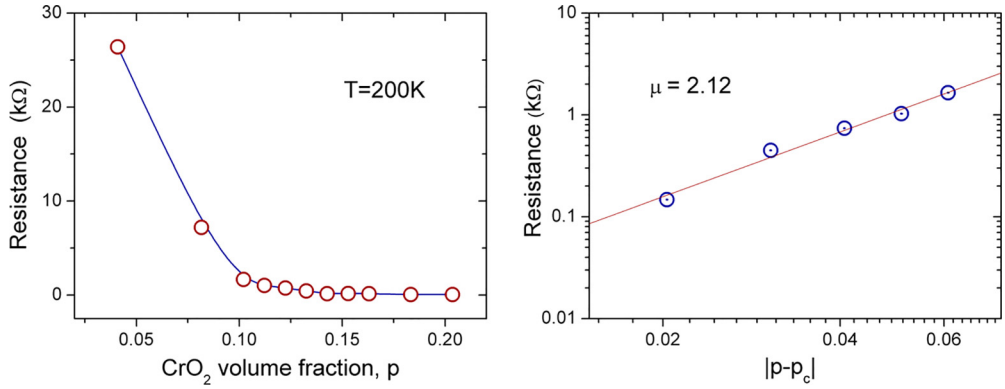

FIG. 7. Left panel: Resistance of the $CrO_2/LiCoO_2$ system as a function of the volume fraction of CrO_2. Right panel: Resistance scaling and the critical exponent μ near the percolation threshold.

$CrO_2/LiCoO_2$ heterointerfaces) to fit into the scaling relation of Eq. (3). The measurements were performed at 200 K to minimize conductivity through the $LiCoO_2$ particles. We determine the percolation threshold to be $p_c = 0.16$ and the critical exponent to be $\mu = 2.12$.

While this value of the critical exponent is very similar to the one obtained for the conductor-insulator transition in the MgB_2/CrO_2 double percolation system, the percolation threshold is significantly lower. Taking into account the filling factor for this system ($f = 0.78$ as we measured), the occupation probability is given by $P_c = 0.125$, in good agreement with the random packing limit for identical particles (the Scher-Zallen value of 0.16 for spheres [39]). In contrast to the MgB_2 percolation described in the previous section, the excluded volume for CrO_2 in the $CrO_2/LiCoO_2$ system is close to the actual volume of the $LiCoO_2$ cylinders [by using Eq. (4) and neglecting the volume of much smaller CrO_2 cylinders], and thus does not significantly alter the percolation threshold.

E. Magnetoresistance effects

To further explore the structure-property relation in the MgB_2/CrO_2 composite system, we measured the resistance of the samples as a function of the magnetic field. We can identify three different volume fraction ranges p in which magnetoresistive effects were observed in these composites. The composites with $p > 0.34$, above the percolation threshold of CrO_2, show a characteristic butterfly-like resistance versus magnetic field curves (not shown), similar to the results obtained in Ref. [9], while composites with MgB_2 volume fraction $p^{MgB_2}=1-p$ above the percolation threshold of MgB_2 (on the superconducting side of the insulator-superconductor transition) show a complex behavior due to the presence of continuous superconducting links, as will be described below.

The most interesting behavior is observed in the intermediate region, i.e., in the range $0.22 < p < 0.34$ when none of the individual components percolate. An example of reversible results of resistance R versus magnetic field H (between -5 T and 5 T) at different temperatures for $p = 0.25$ (near the maximum of the resistivity peak) is shown in Fig. 8. At high enough temperature (>25 K), the resistance curves are of the characteristic butterfly shape as well, as shown on the right panels of Fig. 8. Our results can be compared with those obtained before for CrO_2 powders which were also cold-pressed in a matrix with antiferromagnetic insulating Cr_2O_3 particles [9], where the characteristic butterfly-shape curves with reversible high-field slope were observed, with the two peaks occurring near the temperature-dependent coercive field. In this case the magnitude of magnetoresistance MR is then defined as $(R_{max} - R_{min})/R_{min}$, where R_{max} is the maximum resistance and the resistance R_{min} is determined by extrapolating the linear part of the curve at large magnetic field to zero field, similarly to the procedure adopted in Ref. [9].

It has been shown that the magnetoresistance in this case might be associated with spin-dependent tunneling via the alignment of the magnetization of CrO_2 particles [9]. For our MgB_2/CrO_2 system here, the maximum magnetoresistance generally occurs at the lowest measurement temperature ($T = 2$ K), as seen in Figs. 9 and 10. However, in contrast to the results of Ref. [9] for CrO_2/Cr_2O_3 powders, the peaks of resistance shown in Fig. 8 do not coincide with the coercivity (∼0.1 T) at temperatures below 35 K (the critical temperature of MgB_2). Moreover, at temperatures below the superconducting transition temperature T_C the position of the peaks shifts toward smaller fields (although the coercivity nominally increases slightly in this temperature range), until the curves become practically nonhysteretic at 2 K and 5 K. This suggests that magnetoresistance at this composition is determined for the most part by the MgB_2/CrO_2 interfaces.

The magnitude of magnetoresistance MR as a function of temperature for different volume fractions of CrO_2 is plotted in Fig. 9, while the MR as a function of volume fraction at different temperatures is plotted in Fig. 10. As can be seen from both figures, the MR of this system has two maxima: One, with MR ≈ 42% at 2 K, is for the sample at $p =$ 0.25, which corresponds to the largest resistance (see Fig. 3); the other of approximately the same MR value corresponds to a much higher fraction of CrO_2, significantly above the percolation threshold, which is consistent with the value of MR = 45% obtained in Ref. [9] for pure CrO_2 powders. We can qualitatively explain this behavior by the interplay of the conductance and magnetoconductance at CrO_2/CrO_2 and CrO_2/MgB_2 interfaces. At high volume fraction of CrO_2 the transport properties of the system are determined for the most part by the CrO_2/CrO_2 interfaces. Below the percolation

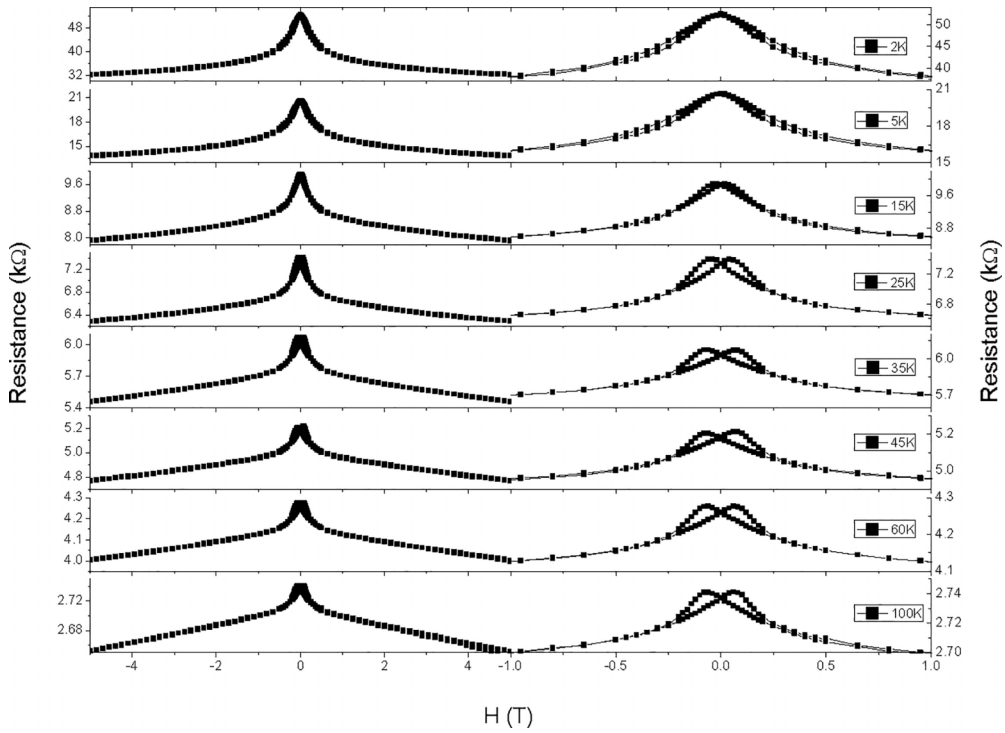

FIG. 8. Resistance of CrO_2/MgB_2 cold-pressed samples below the MgB_2 percolation threshold (at $p = 0.25$) as a function of magnetic field H at different temperatures. Left: Full range of magnetic field ranging from -5 T to 5 T. Right: Blow up of the central region (from -1 T to 1 T), with the characteristic butterfly-shape magnetoresistance curves appearing above 15 K.

threshold of CrO_2 "infinite" cluster of CrO_2 is no longer present in this double percolation system (see Sec. III A), so that the conductance is beginning to be strongly influenced by the CrO_2/MgB_2 interfaces, which have significantly higher contact resistance at low temperatures. As the fraction of MgB_2 increases (i.e., p decreases) further and the number of CrO_2/MgB_2 interfaces increases, the MR of the composite becomes commensurate with the resistance, reaching a maximum at $p = 0.25$ which corresponds to the highest resistance of the system (as shown in Fig. 3). This picture is consistent with the fact that the increase of MR near $p = 0.25$ as the temperature is lowered has the fastest rate compared to all other compositions (see Fig. 9), emphasizing the role of S/F interfaces and the coupling between the magnetoresistance effect and double percolation transition.

While the maximum values of MR = 42% in our composite system at 2 K (see Fig. 10) is comparable to the results of Ref. [9], we believe that the origin of this magnetoresistance near $p = 0.25$ is very different. Indeed, while the value of the upper critical field H_{c2}, obtained from our resistivity

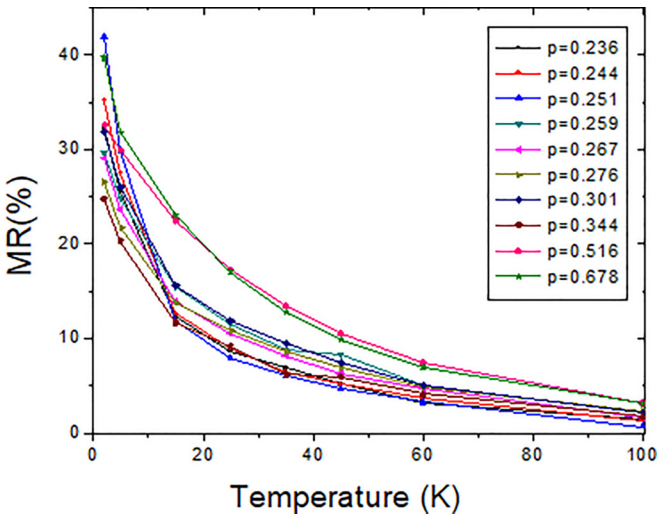

FIG. 9. Temperature dependence of the magnitude of magnetoresistance for CrO_2/MgB_2 composites with $p > 0.23$.

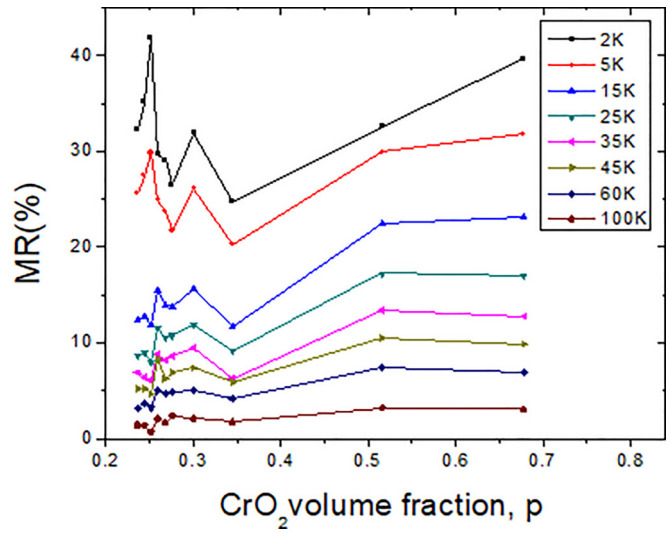

FIG. 10. Magnitude of magnetoresistance for the CrO_2/MgB_2 samples with volume fraction $p > 0.24$ at different temperatures.

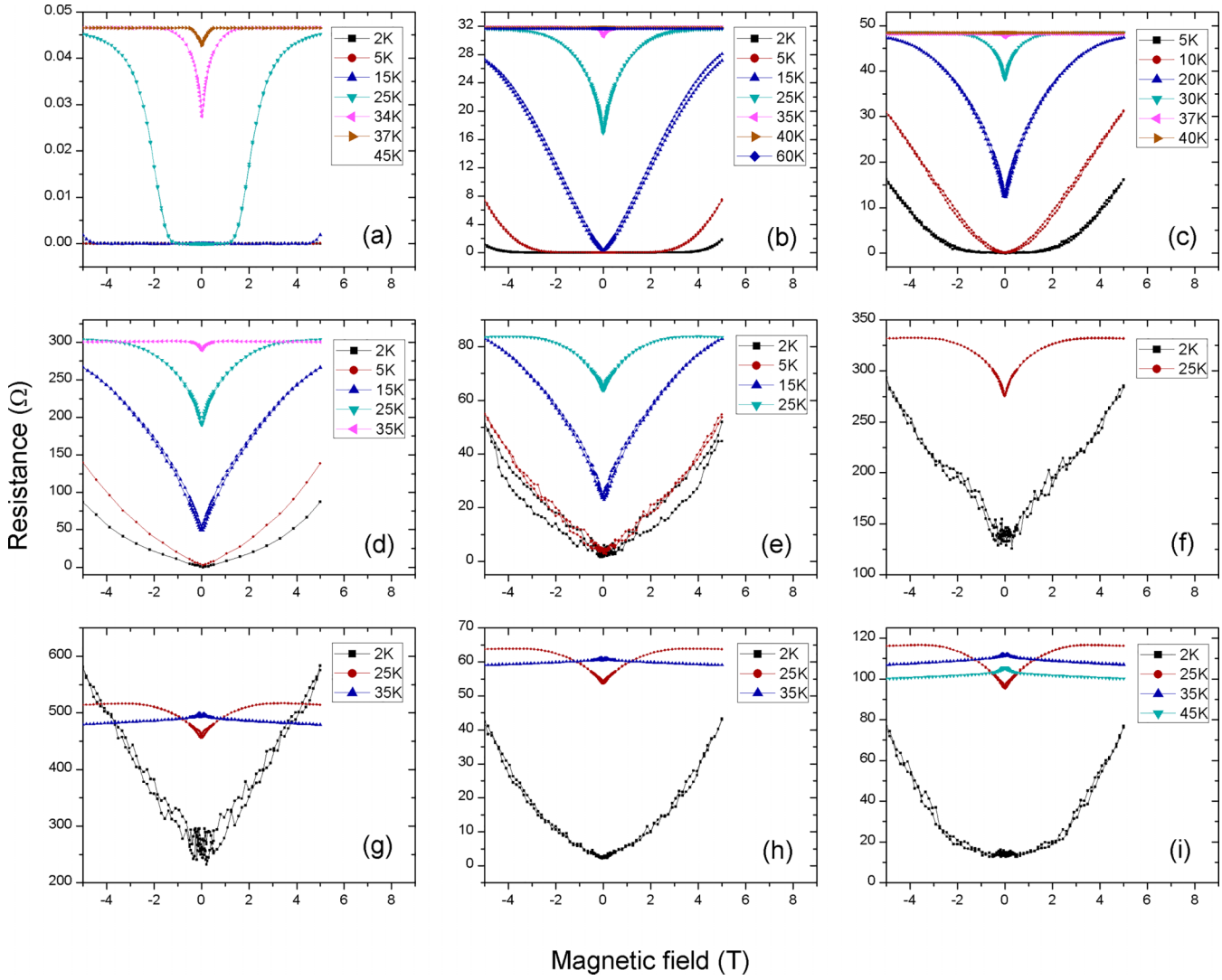

FIG. 11. Magnetic-field-dependent resistance of $(CrO_2)_p(MgB_2)_{1-p}$ cold-pressed samples for $p = 0$, 0.055, 0.150, 0.177, 0.198, 0.205, 0.213, 0.221, and 0.228 in panels (a–i), respectively.

measurements for pure MgB_2 samples, was about 6 T at 5 K (at 2K it exceeded the maximum field we could apply in our PPMS/MPMS systems), the first critical field H_{c1} is known to be quite low, with vortices observed at magnetic fields on the order of mT [47]. As a result, a certain field-dependent fraction of MgB_2 surface area has a modified electronic structure with strongly suppressed superconductivity even at relatively low fields [19], influencing the Andreev reflection amplitudes, which affects the resistance of the MgB_2/CrO_2 contacts, reducing the overall resistance of the composite sample. In a field on the order of 100 mT, comparable to the coercivity of CrO_2 [15]. The distance d between vortices in a type II superconductor can be estimated to be on the order of 100 nm. This implies that at least several vortices are present within a single MgB_2 nanoparticle, with the number averaging out over the current path. This, in turn makes it possible to introduce a "parallel resistance" model, which was evaluated in the point contact Andreev reflection (PCAR) measurements of MgB_2 in a variable magnetic field [48]. While it may be possible to study the effect quantitatively, it is not easy due to the two-band structure (σ, π) of MgB_2 which have different coherence lengths and other parameters [48] and is beyond the scope of this work. Qualitatively, though, we note that our simple model explains the absence of hysteresis at the lowest temperatures, where the Andreev reflection effects in MgB_2/CrO_2 junctions dominate the overall resistance. A very small hysteresis is still present, likely due to a stray magnetic field from CrO_2 nanoparticles. At higher temperatures when the CrO_2/CrO_2 junctions are beginning to play a progressively more important role in the overall resistance, the hysteresis gradually appears, in agreement with the finding of Ref. [9]. Similarly, the sharpness of the MR peak (as a function of volume fraction; see Fig. 10) is maximized near $p = 0.25$, which corresponds to the largest resistance and hence the largest number of MgB_2/CrO_2 junctions.

A different type of magnetoresistance is observed in samples for which the MgB_2 volume fraction is above the MgB_2 percolation threshold (i.e., smaller p and larger $1 - p > p_c^{MgB_2}$). A typical magnetic-field dependence of resistance is presented in Fig. 11. The sample resistance increases with magnetic field at various temperatures, showing positive magnetoresistance, in contrast to the negative magnetoresistance

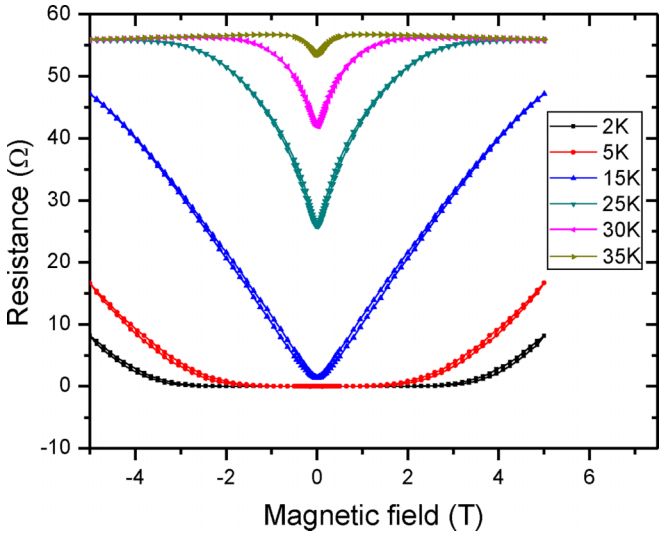

FIG. 12. Results of resistance vs magnetic field for $(LSMO)_{0.8}(MgB_2)_{0.2}$ sample at different temperatures.

for the volume fraction of MgB_2 below its percolation threshold as described above. Interestingly, larger volume fraction of MgB_2 (smaller p) corresponds to higher maximum temperature at which the positive magnetoresistance can be observed; e.g., for a pure MgB_2 sample ($p = 0$), positive magnetoresistance is observed up to 37 K, while for samples of lower MgB_2 concentration (larger p) positive magnetoresistance is observed only below 25 K, which may be related to the increased influence of the magnetic phase (CrO_2).

A similar phenomenon of positive magnetoresistance has been observed by Barber and Dynes [49], who investigated granular Pb films near the insulator-superconductor transition in a magnetic field. They described three regimes corresponding to this behavior. At magnetic fields higher than some crossover point H_x, a power-law behavior $R \propto H^{\alpha}$ was found for intermediate fields, while at higher magnetic fields a logarithmic behavior $R \propto \log H$ was observed. The authors related the crossover field H_x to the size of the regions of superconducting phase coherence, which increases with the average grain thickness. In our case here, a similar scenario may take place, that is, more MgB_2 particles are needed to achieve global coherence.

We note that for the concentration range very close to the MgB_2 threshold, hysteretic behavior has been repeatedly observed at the lowest measurement temperature (~2 K) [see Figs. 11(e)–11(i)]. We speculate that this behavior might be related to the vortex motion in MgB_2, although more systematic studies are needed to confirm this assumption. Qualitatively similar effects have also been observed in the $(LSMO)_p(MgB_2)_{1-p}$ composite system. In Fig. 12 the magnetic-field-dependent resistance curves for $(LSMO)_{0.61}(MgB_2)_{0.39}$ are presented, showing the behavior analogous to that for $(CrO_2)_p(MgB_2)_{1-p}$ samples presented in Fig. 11.

IV. CONCLUSIONS

We have investigated a number of two-component nanoparticle percolation systems, the complex behavior of which is controlled by their functional properties, such as interface tunneling between the superconducting and ferromagnetic nanoparticles, as well as their geometric properties such as size and/or shape disparity, as demonstrated by our results of CrO_2/MgB_2, Cr_2O_3/MgB_2, $LSMO/MgB_2$, and $CrO_2/LiCoO_2$ composite systems. Compared to the CrO_2/MgB_2 double percolation composite showing anomalously large threshold for MgB_2 percolation (with volume fraction $p_c^{MgB_2} = 0.78$), replacing CrO_2 particles with ferromagnetic and approximately spherical LSMO particles resulted in a much smaller average percolation threshold $p_c \approx 0.35$. However, replacing roughly spherical MgB_2 particles by large cylindrical $LiCoO_2$ particles resulted in a low percolation threshold for CrO_2, with volume fraction $p_c = 0.16$.

The effect of particle geometry disparity, combined with the effectively blocked conductance path between different types of constituent particles, is directly responsible for the double percolation transition observed in the CrO_2/MgB_2 system, resulting in a conductor-insulator-superconductor crossover effect. Each of the CrO_2- and MgB_2-dominated percolative transitions is essentially different from the conventional percolation transitions for a single type of particles involving conducting or superconducting states, resulting in a similar but different form of scaling behavior for the sample resistance near each percolation threshold when $p < p_c$ (instead of $p > p_c$ conventionally) in our unconventional binary composite systems. Our simple model can explain the anomalously high threshold observed for the spherical MgB_2 particles, which is directly related to the large geometric contrast of the constituent particles and the corresponding excluded volume of highly anisotropic CrO_2 sticks. We have also found the link between the maximum filling factor for the CrO_2/MgB_2 composite and the percolation threshold for CrO_2, as well as a power-law behavior of the filling factor, indicating the presence of geometric phase transition in this system.

Using the range of volume fractions $0.22 < p < 0.34$ we were able to isolate the contributions of CrO_2/MgB_2 junctions to electrical conductivity of the composite system. This, in turn, made it possible to directly measure the effects of nonhysteretic magnetoresistance at the half-metal/superconductor interface, where a partial suppression of superconductivity in a Type II two-gap superconductor (MgB_2) leads to the *decrease* of the junction resistance [13]. The low-temperature MR values are very sensitive to minute variations of composition near the resistance maximum, with the highest MR ~ 42% at liquid helium temperatures obtained at volume fraction $p = 0.25$ between the two percolation thresholds.

The approach presented here can be applied to other material systems to provide an effective avenue for understanding the nontrivial connection between material functionality and the structure or geometry of its constituents, which is especially important for multi-component systems. Another implication of this study is the possibility of controlling the system properties by adjusting various geometric factors (size, shape, anisotropy, etc.) of the constituent particles, to realize different system modes important for materials applications (e.g., conducting-insulating-superconducting crossover as demonstrated here). For example, one may be able to adjust

the percolation thresholds by varying the size of one (or both) of the constituent particles to facilitate a convergence of the nonpercolative segment in the composition-resistance phase diagram to a single point, so that the resistance of such a system will become essentially bimodal, a useful property for various device applications.

ACKNOWLEDGMENTS

We thank R. Seshadri and A. Gurevich for discussions and many useful suggestions and Brendon Waters for his help in preparing the illustration used in Fig. 3. The work at Wayne State was supported by the National Science Foundation under Grants No. ECS-0239058, No. DMR-1006381, and No. DMR-2117487 (B.N.) and Grant No. DMR-2006446 (Z.-F.H.). The UCSB-LANL Institute for Multiscale Materials Studies, the National Science Foundation (Grant No. DMR-0449354), and the use of MRL Central Facilities, supported by the MRSEC Program of the NSF (Grant No. DMR05-20415), a member of the NSF-funded Materials Research Facilities Network [50], are gratefully acknowledged (D.P.S.).

[1] J. S. Moya, S. Lopez-Esteban, and C. Pecharroman, The challenge of ceramic/metal microcomposites and nanocomposites, Prog. Mater. Sci. **52**, 1017 (2007).

[2] D. Stauffer and A. Aharony, *Introduction to Percolation Theory* (Taylor & Francis, London, 1994).

[3] M. Imada, A. Fujimori, and Y. Tokura, Metal-insulator transitions, Rev. Mod. Phys. **70**, 1039 (1998).

[4] S. Alexander, Superconductivity of networks. A percolation approach to the effects of disorder, Phys. Rev. B **27**, 1541 (1983).

[5] Y. M. Strelniker, A. Frydman, and S. Havlin, Percolation model for the superconductor-insulator transition in granular films, Phys. Rev. B **76**, 224528 (2007).

[6] R. Mezzenga, J. Ruokolainen, G. H. Fredrickson, E. J. Kramer, D. Moses, A. J. Heeger, O. Ikkala, Templating organic semiconductors via self-assembly of polymer colloids, Science **299**, 1872 (2003).

[7] A. Yamamoto, A. Ishihara, M. Tomita, and K. Kishio, Permanent magnet with MgB_2 bulk superconductor, Supercond. Sci. Technol. **20**, 658 (2007).

[8] M. Eisterer, M. Zehetmayer, and H. W. Weber, Current Percolation and Anisotropy in Polycrystalline MgB_2, Phys. Rev. Lett. **90**, 247002 (2003).

[9] J. M. D. Coey, A. E. Berkowitz, L. Balcells, and F. F. Putris, Magnetoresistance of Chromium Dioxide Powder Compacts, Phys. Rev. Lett. **80**, 3815 (1998).

[10] R. Mukherjee, G. Lawes, and B. Nadgorny, Enhancement of high dielectric permittivity in $CaCu_3Ti_4O_{12}/RuO_2$ composites in the vicinity of the percolation threshold, Appl. Phys. Lett. **105**, 072901 (2014).

[11] Z. Rubin, S. A. Sunshine, M. B. Heaney, I. Bloom, and I. Balberg, Critical behavior of the electrical transport properties in a tunneling-percolation system, Phys. Rev. B **59**, 12196 (1999).

[12] X. Liu, R. P. Panguluri, Z.-F. Huang, and B. Nadgorny, Double Percolation Transition in Superconductor-Ferromagnet Nanocomposites, Phys. Rev. Lett. **104**, 035701 (2010).

[13] B. Nadgorny and I. I. Mazin, High efficiency nonvolatile ferromagnet/superconductor switch, Applied Physics Letters **80**, 3973 (2002).

[14] I. Žutić, A. Matos-Abiague, B. Scharf, H. Dery, and K. Belashchenko, Proximitized materials, Mater. Today **22**, 85 (2019).

[15] A. E. Berkowitz, J. R. Mitchell, M. J. Carey, A. P. Young, S. Zhang, F. E. Spada, F. T. Parker, A. Hutten, and G. Thomas, Giant Magnetoresistance in Heterogeneous Cu-Co Alloys, Phys. Rev. Lett. **68**, 3745 (1992).

[16] J. M. D. Coey and M. Venkatesan, Half-metallic ferromagnetism: Example of CrO_2 (invited), J. Appl. Phys. **91**, 8345 (2002).

[17] J. Dai and J. Tang, Characterization of the natural barriers of intergranular tunnel junctions: Cr_2O_3 surface layers on CrO_2 nanoparticles, Appl. Phys. Lett. **77**, 2840 (2000).

[18] E. Y. Beliayev, V. A. Horielyi, and Y. A. Kolesnichenko, Magnetotransport properties of CrO_2 powder composites (Review article), Low Temp. Phys. **47**, 355 (2021).

[19] M. R. Eskildsen, M. Kugler, S. Tanaka, J. Jun, S. M. Kazakov, J. Karpinski, and O. Fischer, Vortex Imaging in the π Band of Magnesium Diboride, Phys. Rev. Lett. **89**, 187003 (2002).

[20] J. Linder and J. W. A. Robinson, Superconducting spintronics, Nat. Phys. **11**, 307 (2015).

[21] Isidoro Martínez, P. Högl, C. González-Ruano, J. P. Cascales, C. Tiusan, Y. Lu, M. Hehn, A. Matos-Abiague, J. Fabian, I. Žutić, and F. G. Aliev, Interfacial Spin-Orbit Coupling: A Platform for Superconducting Spintronics, Phys. Rev. Appl. **13**, 014030 (2020).

[22] R. Cai, Y. Yao, P. Lv, Y. Ma, W. Xing, B. Li, Y. Ji, H. Zhou, C. Shen, S. Jia *et al.*, Evidence for anisotropic spin-triplet Andreev reflection at the 2D van der Waals ferromagnet/superconductor interface, Nat. Commun. **12**, 6725 (2021).

[23] J. Nagamatsu, N. Nakagawa, T. Muranaka, Y. Zenitani, and J. Akimitsu, Superconductivity at 39 K in magnesium diboride, Nature (London) **410**, 63 (2001).

[24] R. A. de Groot, F. M. Mueller, P. G. van Engen, and K. H. J. Buschow, New Class of Materials: Half-Metallic Ferromagnets, Phys. Rev. Lett. **50**, 2024 (1983).

[25] B. Nadgorny, I. I. Mazin, M. Osofsky, R. J. Soulen, Jr., P. Broussard, R. M. Stroud, D. J. Singh, V. G. Harris, A. Arsenov, and Ya. Mukovskii, Origin of high transport spin polarization in $La_{0.7}Sr_{0.3}MnO_3$: Direct evidence for minority spin states, Phys. Rev. B **63**, 184433 (2001).

[26] J. F. Berar and G. Baldinozzi, Xnd code from X-ray laboratory data to incommensurately modulated phases. Rietveld modelling of complex materials, International Union of Crystallography, Newsletter No. 20 (1998), https://www.iucr.org/resources/commissions/powder-diffraction.

[27] J. M. Normand and H. J. Herrmann, Precise determination of the conductivity exponent of 3d percolation using "Percola, Int. J. Mod. Phys. C **06**, 813 (1996).

[28] A. Bunde and W. Dieterich, Investigation of electrical stability of nonwovens with conductive circuits using printed conductive inks, J. Electroceram. **5**, 81 (2000).

[29] J. Bernasconi, Classical diffusion in one-dimensional disordered lattice, Phys. Rev. B **18**, 2185 (1978); H. J. Herrmann, B. Derrida, and J. Vannimenus, Superconductivity exponents in two- and three-dimensional percolation, *ibid.* **30**, 4080 (1984).

[30] R. J. Soulen, Jr., J. M. Byers, M. S. Osofsky, B. Nadgorny, T. Ambrose, S. F. Cheng, P. R. Broussard, C. T. Tanaka, J. Nowak, J. S. Moodera, A. Barry, and J. M. D. Coey, Measuring the spin polarization of a metal with a superconducting point contact, Science **282**, 85 (1998).

[31] I. Žutić and S. Das Sarma, Spin-polarized transport and Andreev reflection in semiconductor/superconductor hybrid structures, Phys. Rev. B **60**, R16322 (1999).

[32] P. Högl, A. Matos-Abiague, I. Žutić, and J. Fabian, Magnetoanisotropic Andreev Reflection in Ferromagnet-Superconductor Junctions, Phys. Rev. Lett. **115**, 116601 (2015).

[33] B. Nadgorny, E. Y. Tsymbal, and I. Žutić, Point contact Andreev reflection spectroscopy, *Spin Transport and Magnetism* (Taylor & Francis, New York, 2011).

[34] L. B. Kiss and P. Svendlindh, New Noise Exponents in Random Conductor-Superconductor and Conductor-Insulator Mixtures, Phys. Rev. Lett. **71**, 2817 (1993), and the references therein.

[35] Y. Bugoslavsky, G. K. Perkins, X. Qi, L. F. Cohen, and A. D. Caplin, Enhancement of the high-magnetic-field critical current density of superconducting MgB_2 by proton irradiation, Nature (London) **410**, 563 (2001); D. Larbalestier, A Gurevich, D. M. Feldmann, A. Polyanskii, High-T_c superconducting materials for electric power applications, *ibid.* **410**, 186 (2001).

[36] A. Serquis, Y. T. Zhu, D. E. Peterson, F. M. Mueller, R. K. Schulze, V. F. Nesterenko, and S. S. Indrakanti, Degradation of MgB_2 under ambient environment, Appl. Phys. Lett. **80**, 4401 (2002).

[37] C. J. Lobb, M. Tinkham, and W. J. Scocpol, Percolation in inhomogeneous superconducting composite wires, Solid State Commun. **27**, 1273 (1978).

[38] S. Pokhrel, B. Waters, S. Felton, Z.-F. Huang, and B. Nadgorny, Percolation in metal-insulator composites of randomly packed spherocylindrical nanoparticles, Phys. Rev. B **103**, 134110 (2021).

[39] H. Scher and R. Zallen, Critical density in percolation processes, J. Chem. Phys. **53**, 3759 (1970).

[40] I. Balberg and N. Binenbaum, Computer study of the percolation threshold in a two-dimensional anisotropic system of conducting sticks, Phys. Rev. B **35**, 8749 (1987).

[41] G. Xiao, F. H. Streitz, M. Z. Cieplak, A. Bakhshai, and A. Gavrin, Electrical transport and superconductivity in a Au-Y percolation system, Phys. Rev. B **38**, 776 (1988).

[42] B. Abeles, H. L. Pinch, and J. Gittleman, Fluctuation-Induced Tunneling Conduction in Carbon-Polyvinylchloride Composites, Phys. Rev. Lett. **35**, 247 (1975).

[43] L. Onsager, The effects of shape on the interaction of colloidal particles, Ann. N.Y. Acad. Sci. **51**, 627 (1949).

[44] A. P. Philipse and S. G. J. M. Kluijtmans, Sphere caging by a random fibre network, Physica A **274**, 516 (1999).

[45] I. Balberg, C. H. Anderson, S. Alexander, and N. Wagner, Excluded volume and its relation to the onset of percolation, Phys. Rev. B **30**, 3933 (1984).

[46] S. I. White, B. A. DiDonna, M. Mu, T. C. Lubensky, and K. I. Winey, Simulations and electrical conductivity of percolated networks of finite rods with various degrees of axial alignment, Phys. Rev. B **79**, 024301 (2009).

[47] J. Karpinski, M. Angst, J. Jun, and S. M. Kazakov, MgB_2 single crystals: High pressure growth and physical properties, Supercond. Sci. Technol. **16**, 221 (2003).

[48] Y. Bugoslavsky, Y. Miyoshi, G. K. Perkins, A. D. Caplin, and L. F. Cohen, A. V. Pogrebnyakov, and X. X. Xi, Electron diffusivities in MgB_2 from point contact spectroscopy, Phys. Rev. B **72**, 224506 (2005).

[49] R. P. Barber, Jr. and R. C. Dynes, Low-field magnetoresistance in granular Pb films near the insulator-superconductor transition, Phys. Rev. B **48**, 10618 (1993).

[50] www.mrfn.org.